*Chin. Ann. Math.*
33B(2), 2012, 225–246
DOI: 10.1007/s11401-012-0701-8

**Chinese Annals of Mathematics, Series B**


# Investigation of Multi-soliton, Multi-cuspon Solutions to the Camassa-Holm Equation and Their Interaction*

Xiaozhou LI[1] Yan XU[2] Yishen LI[1]

**Abstract** The authors study the multi-soliton, multi-cuspon solutions to the Camassa-Holm equation and their interaction. According to the solution formula due to Li in 2004 and 2005, the authors give the proper choice of parameters for multi-soliton and multi-cuspon solutions, especially for $n \geq 3$ case. The numerical method (the so-called local discontinuous Galerkin (LDG) method) is also used to simulate the solutions and give the comparison of exact solutions and numerical solutions. The numerical results for the two-soliton and one-cuspon, one-soliton and two-cuspon, three-soliton, three-cuspon, three-soliton and one-cuspon, two-soliton and two-cuspon, one-soliton and three-cuspon, four-soliton and four-cuspon are investigated by the numerical method for the first time, respectively.

**Keywords** Camassa-Holm equation, Local discontinuous Galerkin method, Multi-soliton, Multi-cuspon
**2000 MR Subject Classification** 65M60, 35Q53

## 1 Introduction

The Camassa-Holm equation

$$u_t - u_{xxt} + 2\omega u_x + 3uu_x = 2u_x u_{xx} + uu_{xxx} \tag{1.1}$$

was proposed in [1–2] as a model for the propagation of the unidirectional gravitational waves in a shallow water approximation, with $u$ representing the free surface of water over a flat bed. This equation has attracted a lot of attention over the past decade due to its interesting mathematical properties, e.g., it is an integrable equation and admits the peakon solution.

In [9] and [10], Li introduced a different approach associated with the Darboux transformation to construct the explicit expressions for multi-soliton solutions. And in [7], Dai and

Manuscript received August 5, 2011. Revised December 16, 2011.
[1]School of Mathematical Sciences, University of Science and Technology of China, Hefei 230026, China. E-mail: guzhou@mail.ustc.edu.cn ysli@ustc.edu.cn
[2]Corresponding author. School of Mathematical Sciences, University of Science and Technology of China, Hefei 230026, China. E-mail: yxu@ustc.edu.cn
*Project supported by the National Natural Science Foundation of China (Nos. 10971211, 11031007), the Foundation for the Author of National Excellent Doctoral Dissertation of China (No. 200916), the Foundation for the Author of National Excellent Doctoral Dissertation of the Chinese Academy of Sciences, Program for New Century Excellent Talents in University of China (No. 09-0922) and the Fundamental Research Funds for the Central Universities (No. WK0010000005).

Li developed this explicit expressions and investigated the interactions of one-soliton and one-cuspon, two-cuspon, two-soliton. ("soliton" — a stable isolated (i.e., solitary) traveling nonlinear wave solution to a set of equations that obeys a superposition-like principle (i.e., solitons maintain their shapes and pass through one another). "cuspon" — nonstandard solitons which differ from peakons in that their wave peaks are cusps (a cusp is a point at which two branches of a curve meet such that the tangent of each branch is equal).) However, they did not obtain the phase shifts after the interactions among soliton and cuspon. When $n, m \geq 3$, the choice of the parameters for $n$-soliton or $m$-cuspon solution is more difficult. In [7], they could not give the parameters for $n, m \geq 3$ case.

The lack of smoothness at the peak of the cuspon introduces high-frequency dispersive errors into the calculation. It is a challenge to find stable and accurate numerical schemes for solving this equation. In [11], Xu and Shu developed a class of local discontinuous Galerkin (LDG) methods for this nonlinear CH equation and proved that their proposed scheme is high-order accurate, nonlinear stable and flexible for arbitrary $h$ and $p$ adaptivity. It was the first provably stable finite element method for the Camassa-Holm equation. The numerical simulation for peakon solutions was investigated in detail in [11]. But they did not provide the numerical simulation for soliton or cuspon solutions.

In this paper, we study the multi-soliton, multi-cuspon solutions to the Camassa-Holm equation and their interaction by using the numerical methods which were developed in [11]. According to the solution formula in [9–10], we give the proper choice of parameters for multi-soliton and multi-cuspon solutions, especially for $n \geq 3$ case. We also use numerical methods (the so-called local discontinuous Galerkin (LDG) method) to simulate the solutions and give the comparison of exact solutions and numerical solutions. To our best knowledge, those interaction phenomena for $n \geq 3$ case have not been found before.

The discontinuous Galerkin (DG) methods we use in this paper are a class of finite element methods using completely discontinuous piecewise polynomial space for the numerical solution and the test functions in the spatial variables. The DG discretization results in an extremely local, element-based discretization, which is beneficial for parallel computing and maintaining high-order accuracy on unstructured meshes. In particular, DG methods are well suited for *hp*-adaptation, which consists of local mesh refinement and/or the adjustment of the polynomial order in individual elements. They also have excellent provable nonlinear stability. The LDG method for the Camassa-Holm equation (1.1) that we design in this paper shares all these nice properties. More general information about DG methods can be found in [3, 5–6, 8]. Recently, Xu and Shu also presented the LDG methods for the Hunter-Saxton equation in [12, 14] and the Degasperis-Procesi equation in [15]. There is a recent review paper on the LDG methods for high-order time-dependent partial differential equations (see [13]), which provides more details.

The paper is organized as follows. In Section 2, we present the formula of multi-soliton and

its extension for the Camassa-Holm equation (1.1). We give some new numerical results for $n \geq 3$ case in Section 3 and Section 4. Concluding remarks are given in Section 5. To make the paper complete, the details of the LDG method in [11] are collected in the Appendix.

## 2 The Explicit Expression of Multi-soliton for the Camassa-Holm Equation

In this section, we will present the formula of multi-soliton and its extension for the Camassa-Holm equation (1.1).

According to [9] and [10], we denote the two fundamental solutions to the KdV spectral problem with a zero potential as

$$\Phi_i(x) = \begin{cases} \cosh(\xi_i), & i = 2k+1, \\ \sinh(\xi_i), & i = 2k, \end{cases} \tag{2.1}$$

$$\xi_i = k_i\Big(y + \frac{\sqrt{\omega}t}{2(k_i^2 - \frac{1}{4\omega})}\Big), \tag{2.2}$$

$$k_i = \frac{\sqrt{1 - \frac{2\omega}{c_i}}}{2\sqrt{\omega}}. \tag{2.3}$$

Then the $n$-soliton solution to the Camassa-Holm equation is given by

$$u(y,t) = \partial_t \ln\Big(\frac{f_1}{f_2}\Big), \tag{2.4}$$

$$f_1 = \frac{W(\Phi_1, \Phi_2, \cdots, \Phi_n, \mathrm{e}^{\frac{y}{2\sqrt{\omega}}})}{W(\Phi_1, \Phi_2, \cdots, \Phi_n)}, \tag{2.5}$$

$$f_2 = \frac{W(\Phi_1, \Phi_2, \cdots, \Phi_n, \mathrm{e}^{\frac{-y}{2\sqrt{\omega}}})}{W(\Phi_1, \Phi_2, \cdots, \Phi_n)}, \tag{2.6}$$

where $W(\Phi_1, \Phi_2, \cdots, \Phi_n)$ is the Wronskian, and the parameter $y$ is related to $x$ through

$$x = \ln\Big(\sqrt{\frac{f_1^2}{f_2^2}}\Big). \tag{2.7}$$

This approach can be extended to $\Phi_1 = \sinh(\xi_1)$, or $\Phi_1 = \cosh(\xi_1)$, $\Phi_2 = \cosh(\xi_2)$, etc. Through this extension, we can get $m$-cuspon solutions and interaction of $n$-soliton and $m$-cuspon. For the above solutions, even when $n = 2$, a few cases can arise, e.g. [7]. But when $n \geq 3$, no theoretical result has been made so far. And in some choices of $\Phi_i$, $c_i \cdots$, the above formula can not get multi-soliton, multi-cuspon solutions (in some cases, even not the solution to Camassa-Holm equation). So how to get an $n$-soliton and $m$-cuspon solution becomes an interesting problem when $n + m \geq 3$.

In the following, we will list the parameter choices for different solutions when $n + m \geq 3$. To our best knowledge, this is the first time to give the discussion for the parameters of the multi-soliton and multi-cuspon solution when $n + m \geq 3$.

(i) **The interaction process $n = 3$**

(a) The interaction of three $\omega$-soliton

$$W(\Phi_1, \Phi_2, \Phi_3) = W(\cosh(\xi_1), \sinh(\xi_2), \cosh(\xi_3)), \quad c_3 > c_2 > c_1 > 0. \tag{2.8}$$

(b) The interaction of three $\omega$-cuspon

$$W(\Phi_1, \Phi_2, \Phi_3) = W(\sinh(\xi_1), \cosh(\xi_2), \sinh(\xi_3)), \quad c_3 < c_2 < c_1 < 0. \tag{2.9}$$

(c) The interaction of one $\omega$-soliton and two $\omega$-cuspon

$$W(\Phi_1, \Phi_2, \Phi_3) = W(\cosh(\xi_1), \sinh(\xi_2), \cosh(\xi_3)), \quad c_3 < 0,\ c_2 < 0,\ c_1 > 0. \tag{2.10}$$

(d) The interaction of two $\omega$-soliton and one $\omega$-cuspon

$$W(\Phi_1, \Phi_2, \Phi_3) = W(\sinh(\xi_1), \cosh(\xi_2), \sinh(\xi_3)), \quad c_3 > 0,\ c_2 > 0,\ c_1 < 0. \tag{2.11}$$

(ii) **The interaction process $n = 4$**

(a) The interaction of four $\omega$-soliton

$$W(\Phi_1, \Phi_2, \Phi_3, \Phi_4) = W(\cosh(\xi_1), \sinh(\xi_2), \cosh(\xi_3), \sinh(\xi_4)), \quad c_4 > c_3 > c_2 > c_1 > 0. \tag{2.12}$$

(b) The interaction of four $\omega$-cuspon

$$W(\Phi_1, \Phi_2, \Phi_3, \Phi_4) = W(\cosh(\xi_1), \sinh(\xi_2), \cosh(\xi_3), \sinh(\xi_4)), \quad c_4 < c_3 < c_2 < c_1 < 0. \tag{2.13}$$

(c) The interaction of one $\omega$-soliton and three $\omega$-cuspon

$$W(\Phi_1, \Phi_2, \Phi_3, \Phi_4) = W(\cosh(\xi_1), \sinh(\xi_2), \sinh(\xi_3), \sinh(\xi_4)), \quad c_1, c_2, c_4 < 0,\ c_3 > 0,\ |c_4| > |c_3| > |c_1| > |c_2|. \tag{2.14}$$

(d) The interaction of two $\omega$-soliton and two $\omega$-cuspon

$$W(\Phi_1, \Phi_2, \Phi_3, \Phi_4) = W(\cosh(\xi_1), \sinh(\xi_2), \cosh(\xi_3), \sinh(\xi_4)), \quad c_1, c_2 > 0,\ c_3, c_4 < 0,\ |c_1| < |c_2| < |c_3| < |c_4|. \tag{2.15}$$

(e) The interaction of three $\omega$-soliton and one $\omega$-cuspon

$$W(\Phi_1, \Phi_2, \Phi_3, \Phi_4) = W(\cosh(\xi_1), \sinh(\xi_2), \sinh(\xi_3), \sinh(\xi_4)), \quad c_1, c_2, c_4 > 0,\ c_3 < 0,\ |c_4| > |c_3| > |c_1| > |c_2|. \tag{2.16}$$

For one $\omega$-soliton, one $\omega$-cuspon and the interaction process $n = 2$, our numerical results can solve the solutions very well. Since these results are the same as the results in [10], we omit these results to save space. We will simulate in detail and report the phenomena of interaction processes when $n = 3$ and $n = 4$.

## 3 The Interaction Processes ($n = 3$)

In this section, we describe the interactions between soliton and cuspon when $n = 3$. We try to find the soliton and cuspon solutions in different cases by extension (2.1)–(2.3) and (2.7) for $n = 3$, and investigate the properties of the solutions. The computational domain is $[-40, 40]$ with periodic boundary conditions for the numerical results in this section.

### 3.1 The interaction of three $\omega$-soliton

We construct the solution by choosing the parameters in (2.8) in the following way:

$$c_1 = 0.3, \quad c_2 = 0.5, \quad c_3 = 0.7, \quad \omega = 0.01.$$

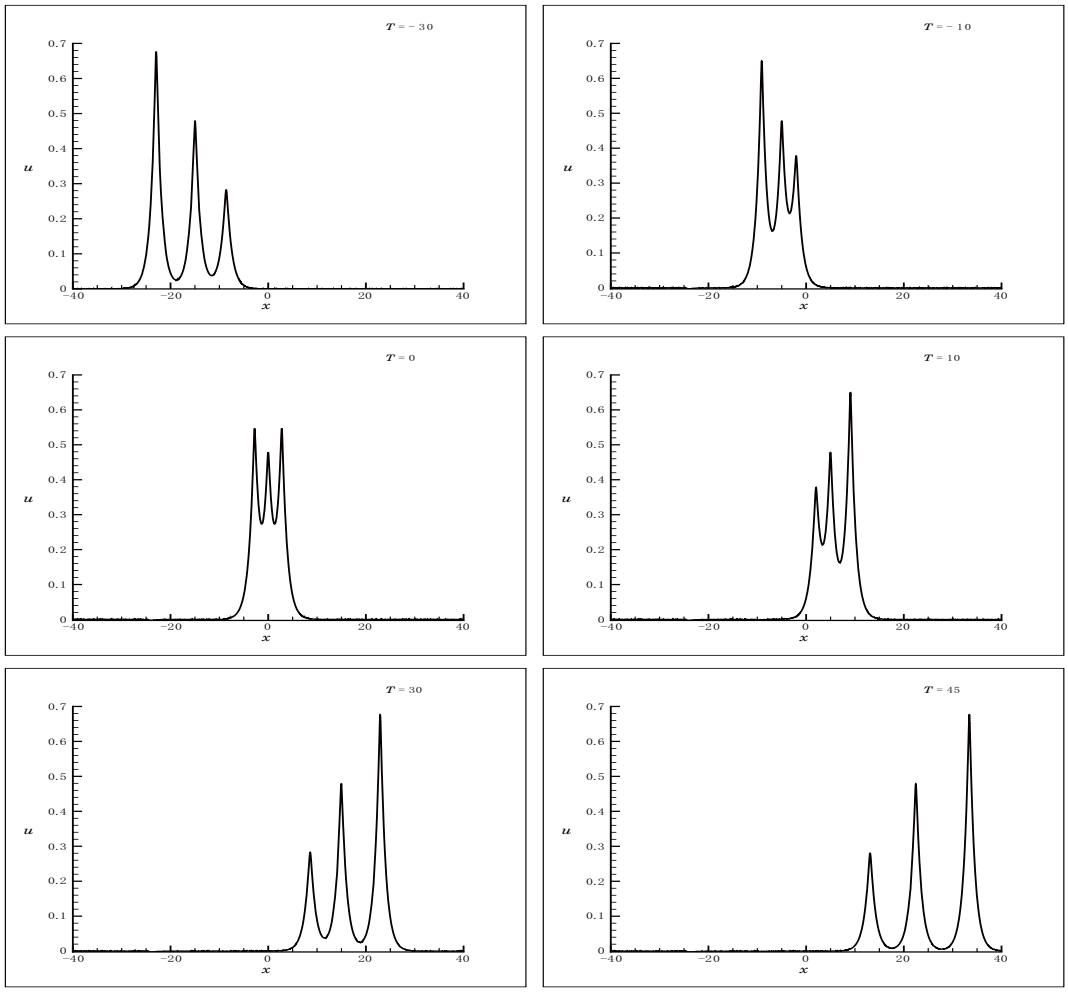


Figure 1 The interaction process of three-soliton solution to the CH equation (1.1) with the initial condition. Periodic boundary condition in $[-40, 40]$. $P^3$ elements and a uniform mesh with 640 cells.

We use the $P^3$ element with $J = 640$ cells in our computation of the LDG method. As shown in Figure 1, we describe the interaction process of three-soliton at different times. We can see clearly that for large $|t|$ the three-soliton solution consists of three moves to the right solitons. Like most cases, the wave with larger amplitude has faster speed. Moreover, note that this description implicity identifies the peaks before and after the collision based on their speeds (or amplitude). However, there is another possible interpretation: the rightmost soliton transfers its energy to the leftmost soliton via the middle soliton without ever overtaking it. This interaction process is very similar to that multi-soliton of KdV equation, except that the three solitons of the Camassa-Holm equation have never merged into a single hump when collision happens. The graph of $\partial_x u(x,t)$ is shown in Figure 2. We also note that the function $\partial_x u(x,t)$ is a continuous function of $x$ and $t$ and further $u(x,t) > 0$.

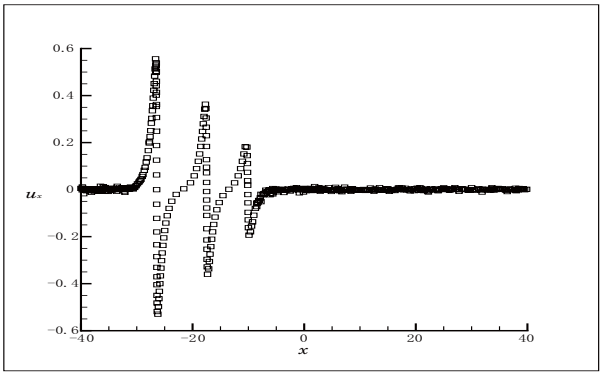


Figure 2 The function $\partial_x u(x,t)$ of three-soliton solution at $T = -35$.

### 3.2 The interaction of three $\omega$-cuspon

We choose the parameters in (2.9) in the following way:

$$c_1 = -0.3, \quad c_2 = -0.5, \quad c_3 = -0.7, \quad \omega = 0.01.$$

We use the $P^3$ element with $J = 1280$ cells in our computation of the LDG method. Figure 3 shows the interaction process at different times. Due to the singularities of the peak of cuspons and their interaction process, they are difficult to be investigated by numerical methods (like classical Finite Element Method, Finite Difference Method). But using local discontinuous Galerkin method which allows discontinuity at the boundary of each element makes it have good perform on dealing those cuspons solution. Actually, no work has been done to study in detail the interaction of three cuspons of the Camassa-Holm equation. We can see that the interaction process has the character very similar to that of the three-soliton process, except that the peaks of each wave are cusps which are shown in Figure 4. This property tells us that the wave is not a standard soliton solution.

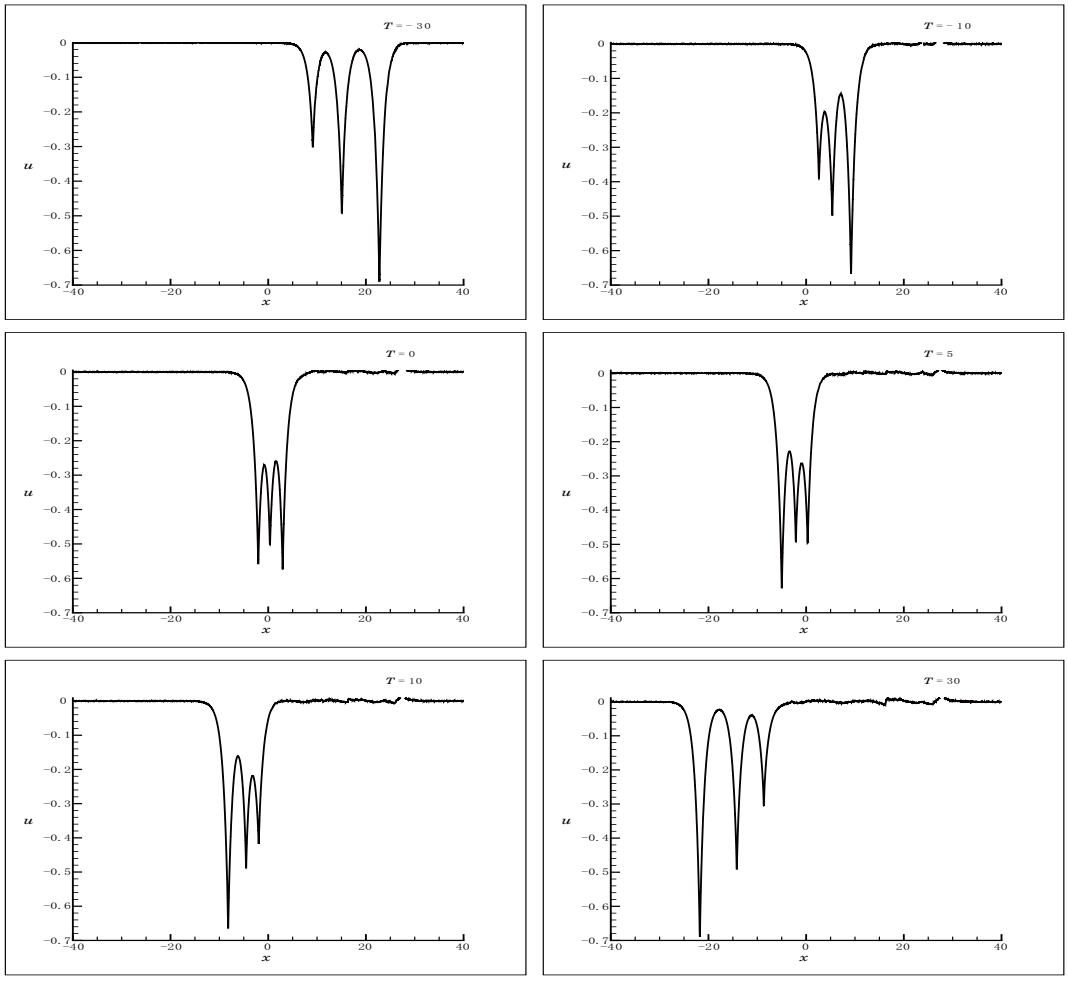


Figure 3 The interaction process of three-cuspon solutions to the CH equation (1.1) with the initial condition. Periodic boundary condition in $[-40, 40]$. $P^3$ elements and a uniform mesh with 1280 cells.

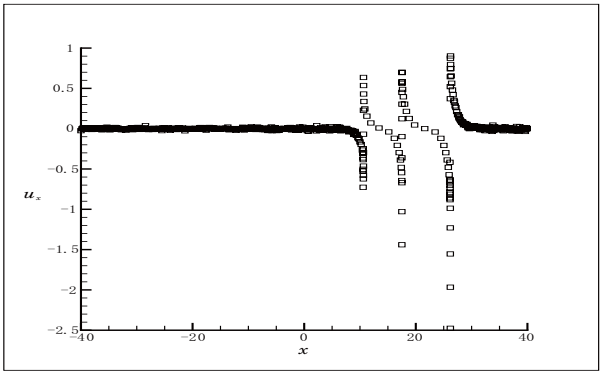


Figure 4 The function $\partial_x u(x,t)$ of three-cuspon solution at $T = -35$.

### 3.3 The interaction of one $\omega$-soliton and two $\omega$-cuspon

We take the parameters in (2.10) in the following way:

$$c_1 = 0.3, \quad c_2 = -0.5, \quad c_3 = -0.7, \quad \omega = 0.01.$$

When $c_3, c_2 < 0,\ c_1 > 0$, the corresponding solution represents the interaction of one-soliton and two-cuspon. When $t \to \infty$, it combines two independent single cuspons and a single soliton. We use the $P^3$ polynomials, each element with $J = 1600$ cells, in our computation of the LDG method. In Figure 5, we describe the interaction process of one-soliton and two-cuspon at different times. We can see that the two cuspon waves have larger amplitude than soliton solution. When the collision happens, all of the three amplitude starts decreasing. At near $t = 0$, it seems like that the cuspons "eat up" the smaller soliton and at almost the same time

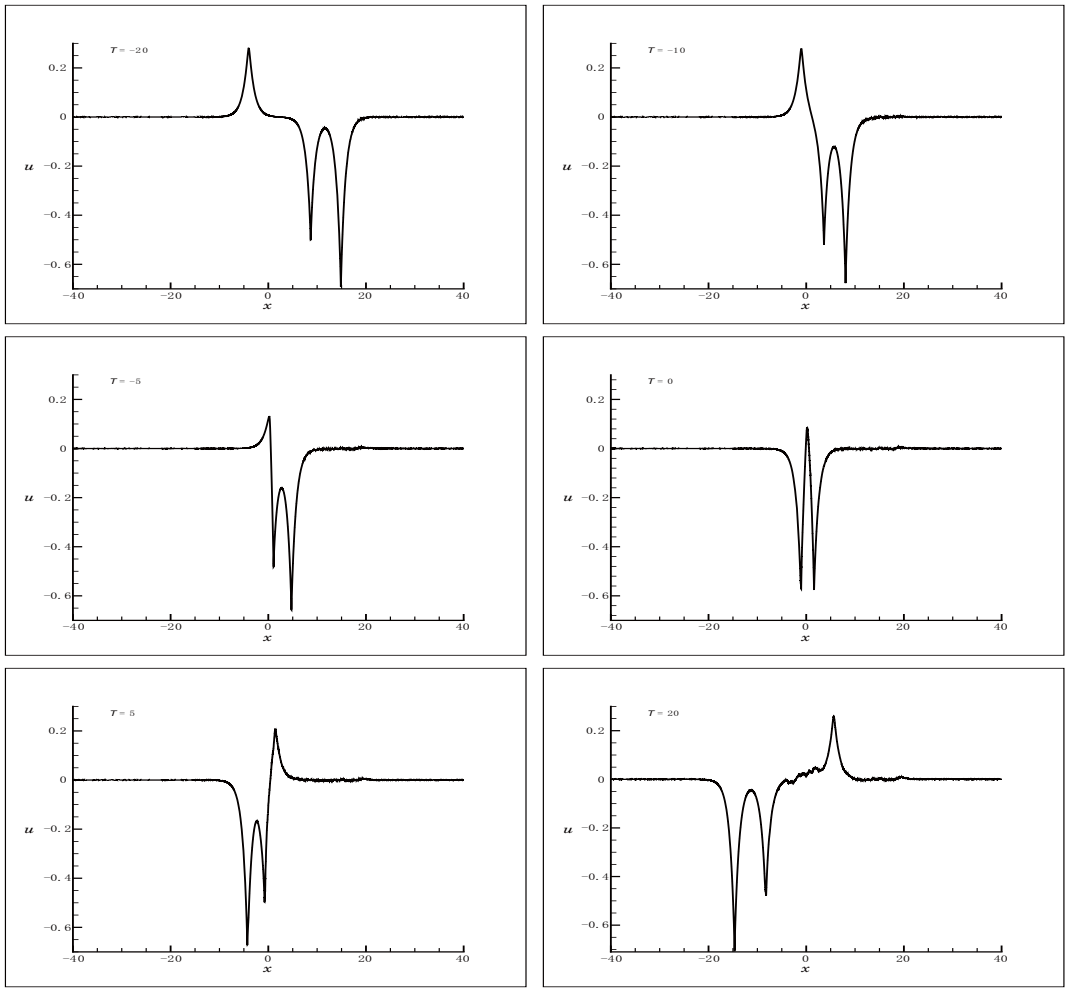


Figure 5 The interaction process of one-soliton and two-cuspon solution to the CH equation (1.1) with the initial condition. Periodic boundary condition in $[-40, 40]$. $P^4$ elements and a uniform mesh with 1600 cells.

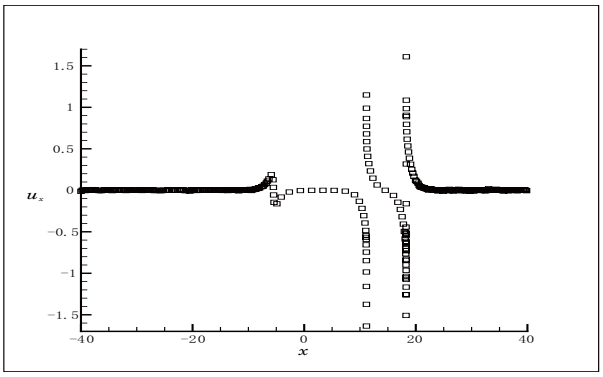


Figure 6 The function $\partial_x u(x,t)$ of one-soliton and two-cuspon solution at $T = -25$.

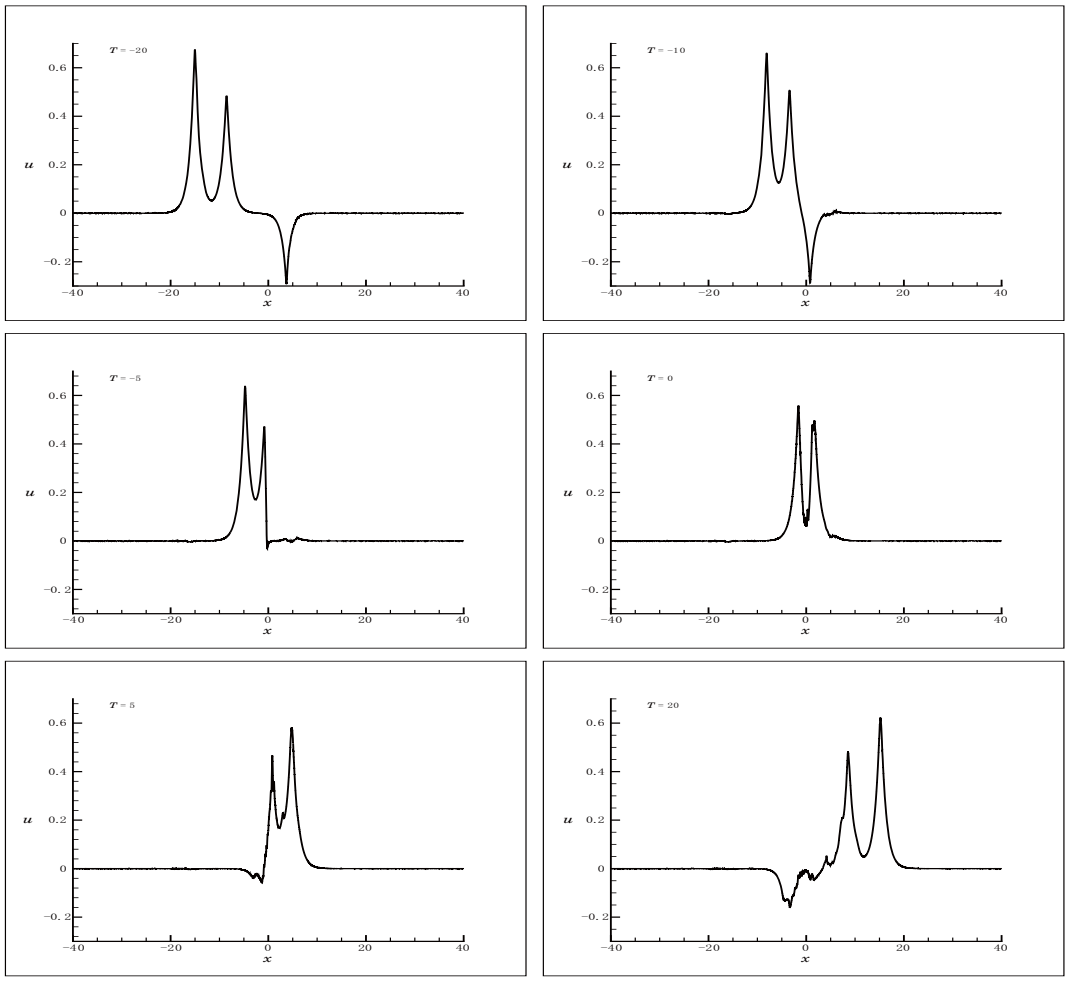


Figure 7 The interaction process of two-soliton and one-cuspon solution to the CH equation (1.1) with the initial condition. Periodic boundary condition in $[-40, 40]$. $P^2$ elements and a uniform mesh with 1280 cells.

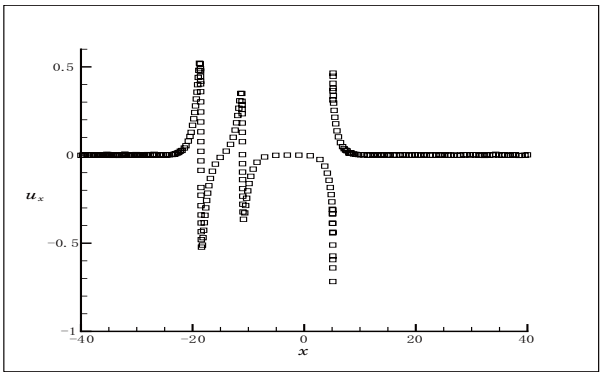


Figure 8 The function $\partial_x u(x,t)$ of two-soliton and one-cuspon solution at $T=-25$.

the faster cuspon catches up the slower cuspon and passes through it. Note that lack of smoothness at the peak of the cuspon and the interaction process cause little numerical oscillation, and the solution curve cannot be plotted very well. This problem can be solved by using more elements or higher order polynomials, but that will cost much more time to compute. By checking $\partial_x u$ in Figure 6, we can identify the soliton and cuspon solutions.

### 3.4 The interaction of two $\omega$-soliton and one $\omega$-cuspon

In (2.11), when $c_3, c_2 > 0,\ c_1 < 0$, the corresponding solution represents the interaction of two-soliton and one-cuspon. We put $c_1 = -0.3,\ c_2 = 0.5,\ c_3 = 0.7$ and $\omega = 0.01$. We use the $P^2$ element with $J = 1280$ cells in our computation of the LDG method. In Figure 7, we describe the interaction process of two-soliton and one-cuspon at different times. The interaction process is very similar to the interaction process of one-soliton and two-cuspon. So we omit the description of this result.

## 4 The Interaction Processes ($n = 4$)

In this section, we describe the interaction between soliton and cuspon when $n = 4$. In a similar way to $n = 3$, we try to find the solutions in different cases by extension (2.1)–(2.3) and (2.7) for $n = 4$, and then investigate the properties of the interaction process by LDG methods. The computational domain is $[-40, 40]$ with periodic boundary conditions for the numerical results in this section.

### 4.1 The interaction of four $\omega$-soliton

We take the parameters in (2.12) as $c_1 = 0.3,\ c_2 = 0.5,\ c_3 = 0.7,\ c_4 = 0.9,\ \omega = 0.01$. When $c_4 > c_3 > c_2 > c_1 > 0$, the corresponding solution is the four-soliton solution. We use the $P^4$ element with $J = 1280$ cells in our computation of the LDG method. As shown in Figure 9, we have plotted the solution profiles for different times which describe the complete interaction

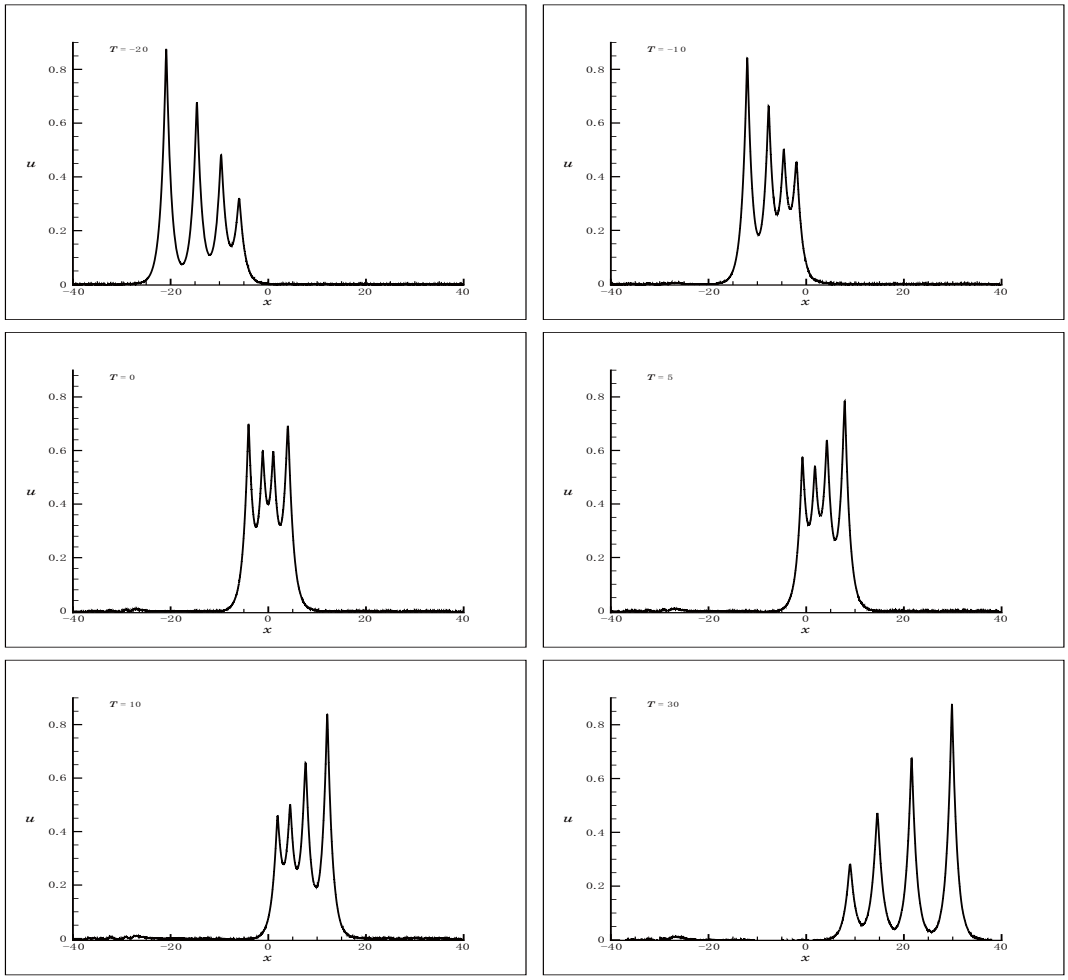


Figure 9 The interaction process of four-soliton solution to the CH equation (1.1) with the initial condition. Periodic boundary condition in $[-40, 40]$. $P^4$ elements and a uniform mesh with 1280 cells.

process of four-soliton. We can see clearly that the wave is a combination of four single solitons when $|t| \to \infty$. Note that at the place where the solitons collide, the faster soliton is shifted forward while the slower soliton is shifted backward. The graph of $\partial_x u(x,t)$ is shown in Figure 10. We also note that the function $\partial_x u(x,t)$ is a continuous function of $x$ and $t$ and further $u(x,t) > 0$.

### 4.2 The interaction of four $\omega$-cuspon

When $c_4 < c_3 < c_2 < c_1 < 0$, the corresponding solution is the three-cuspon solution. We choose the parameters in (2.13) as

$$c_1 = -0.3, \quad c_2 = -0.5, \quad c_3 = -0.7, \quad c_4 = -0.9, \quad \omega = 0.01.$$

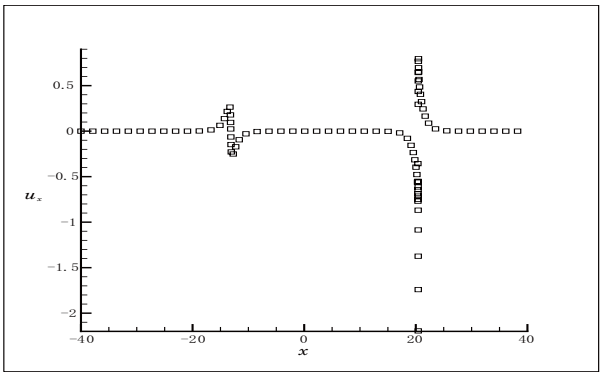


Figure 10 The function $\partial_x u(x,t)$ of four-soliton solution at $T=-25$.

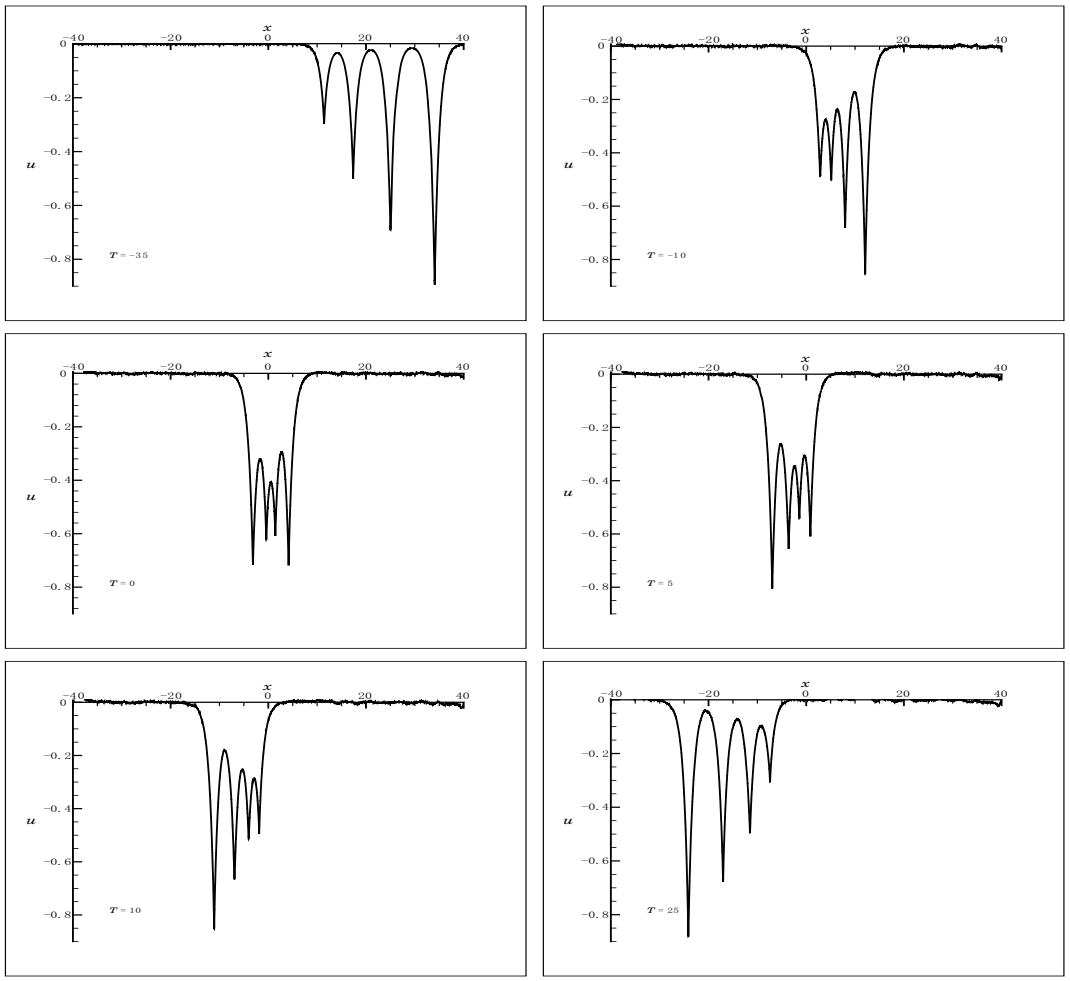


Figure 11 The interaction process of four-cuspon solution to the CH equation (1.1) with the initial condition. Periodic boundary condition in $[-40,40]$. $P^4$ elements and a uniform mesh with 1280 cells.

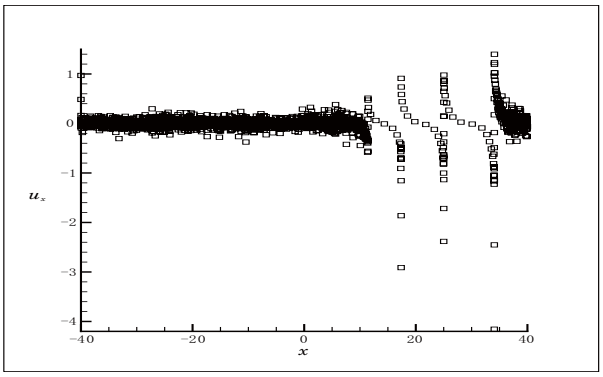


Figure 12 The function $\partial_x u(x,t)$ of four-cuspon solution at $T=-35$.

We use the $P^4$ element with $J=1280$ cells in our computation of the LDG method. Figure 11 shows the interaction process at different times. We can see that the interaction process has the character very similar to that of the three-soliton case, except that the peaks of each wave are cusps which can be seen by checking the function $\partial_x u$ shown in Figure 12.

### 4.3 The interaction of one $\omega$-soliton and three $\omega$-cuspon

We choose the parameters in (2.14) in the following way:

$$c_1=-0.5,\quad c_2=-0.3,\quad c_3=0.7,\quad c_4=-0.9,\quad \omega=0.01.$$

When $c_1,c_2,c_4<0,\ c_3>0,\ |c_4|>|c_3|>|c_1|>|c_2|$, the corresponding solution represents the interaction of one-soliton and three-cuspon. We use the $P^5$ element with $J=1280$ cells in our computation of the LDG method. In Figure 13, we represent the interaction process of one-soliton and three-cuspon. We can see that the only soliton has amplitude at the second place. When the collision happens, all of the three amplitude starts decreasing. At near $t=0$, it seems like that the largest cuspon "eats up" the smaller soliton and at almost the same time, the faster cuspon catches up the slower cuspon and passes through it. And different from the interaction process of one-soliton and two-cuspon we have given in the previous section, the amplitude of soliton is not the smallest one, so during the collision it also "eats up" a smaller cuspon, so we only see two peaks at the time near $t=0$. Again numerical oscillations appear. But those oscillations do not affect our observation of the properties of the interaction process. To plot the solution curve better, we can refine the grids and use a higher order scheme, but those have not been done because of the time cost.

### 4.4 The interaction of two $\omega$-soliton and two $\omega$-cuspon

When $c_1,c_2>0,\ c_3,c_4<0,\ |c_1|<|c_2|<|c_3|<|c_4|$, the corresponding solution represents the interaction of two-soliton and two-cuspon. We put $c_1=0.3,\ c_2=0.5,\ c_3=-0.7,\ c_4=-0.9$ and $\omega=0.01$ in (2.15). We use the $P^4$ element with $J=1600$ cells in our computation of the

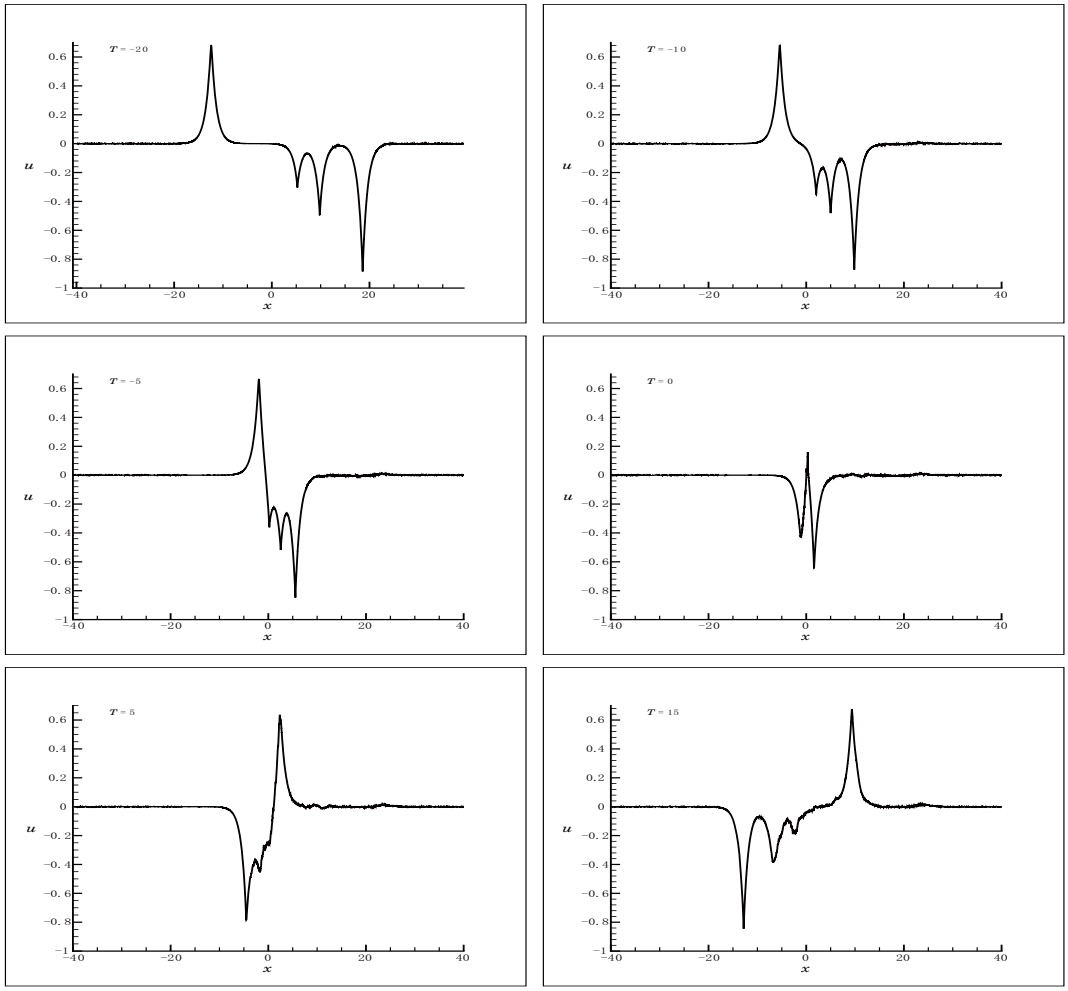


Figure 13 The interaction process of one-soliton and three-cuspon solution to the CH equation (1.1) with the initial condition. Periodic boundary condition in $[-40, 40]$. $P^5$ elements and a uniform mesh with 1280 cells.

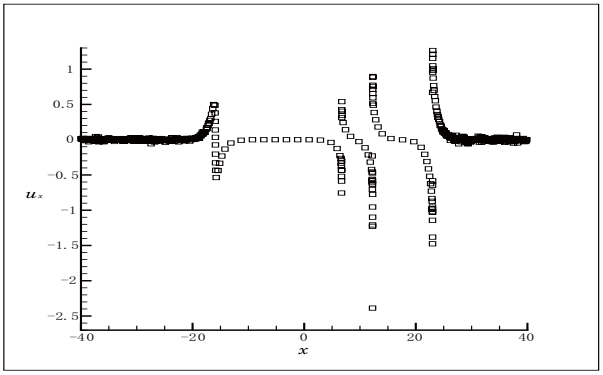


Figure 14 The function $\partial_x u(x,t)$ of one-soliton and three-cuspon solution at $T = -25$.

LDG method. In Figure 15, we use serval plots at different times to describe the complete interaction process of two-soliton and two-cuspon. By checking $\partial_x u$ in Figure 16, we know that the two peaks with smaller amplitude represent two solitons, and the larger two are cuspons. During the collision process, as the soliton-cuspon collision results shown in the previous section, the larger cuspons have "eaten up" the smaller solitons. So at $t = 0$, we only see two peaks appear.

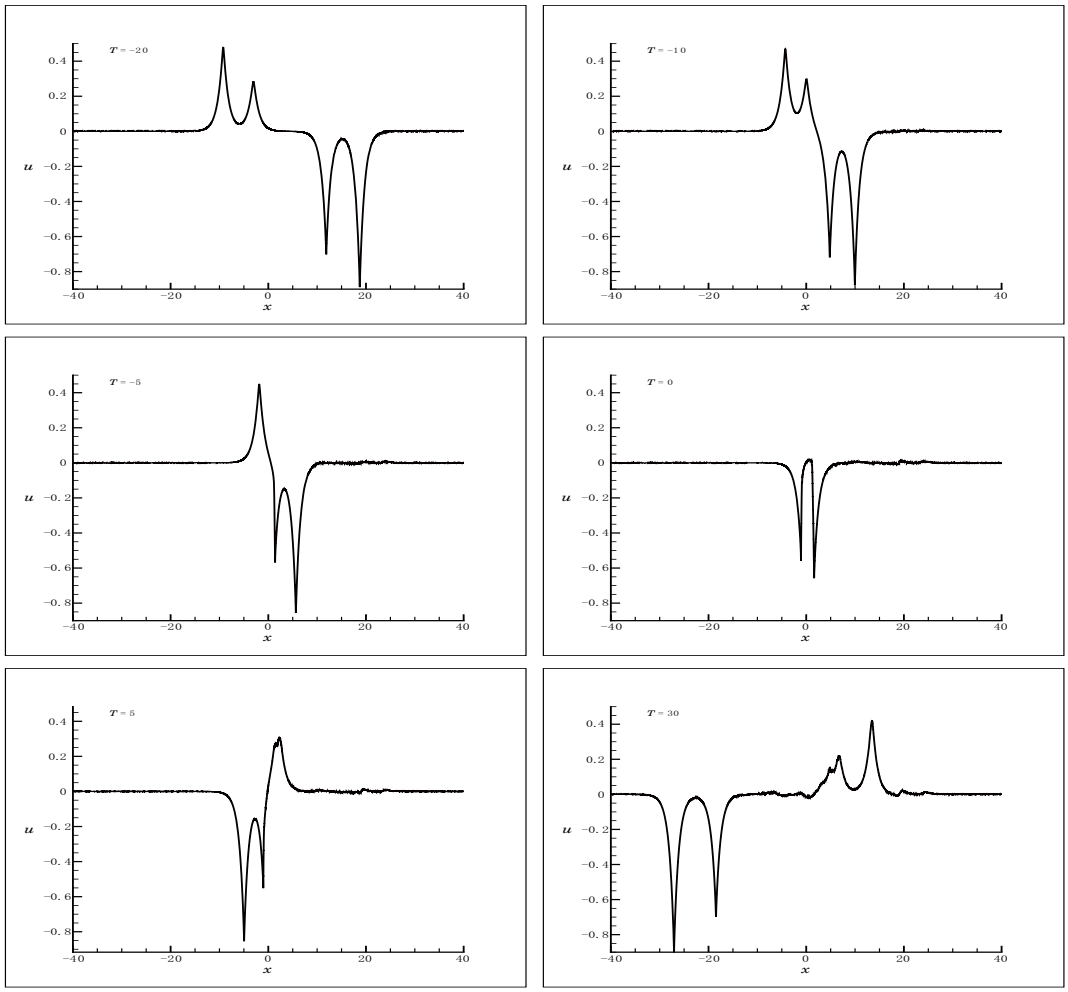


Figure 15 The interaction process of two-soliton and two-cuspon solution to the CH equation (1.1) with the initial condition. Periodic boundary condition in $[-40, 40]$. $P^4$ elements and a uniform mesh with 1600 cells.

### 4.5 The interaction of three $\omega$-soliton and one $\omega$-cuspon

We choose the parameters in (2.16) in the following way: $c_1 = 0.5$, $c_2 = 0.3$, $c_3 = -0.7$, $c_4 = 0.9$, $\omega = 0.01$. When $c_1, c_2, c_4 > 0$, $c_3 < 0$, $|c_4| > |c_3| > |c_1| > |c_2|$, the corresponding solution represents the interaction of three-soliton and one-cuspon. We use the $P^4$ element

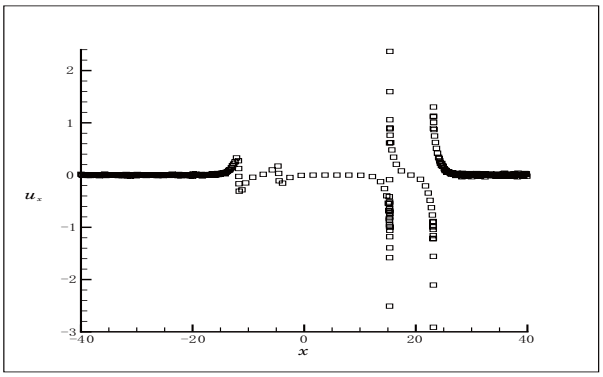


Figure 16 The function $\partial_x u(x,t)$ of two-soliton and two-cuspon solution at $T=-25$.

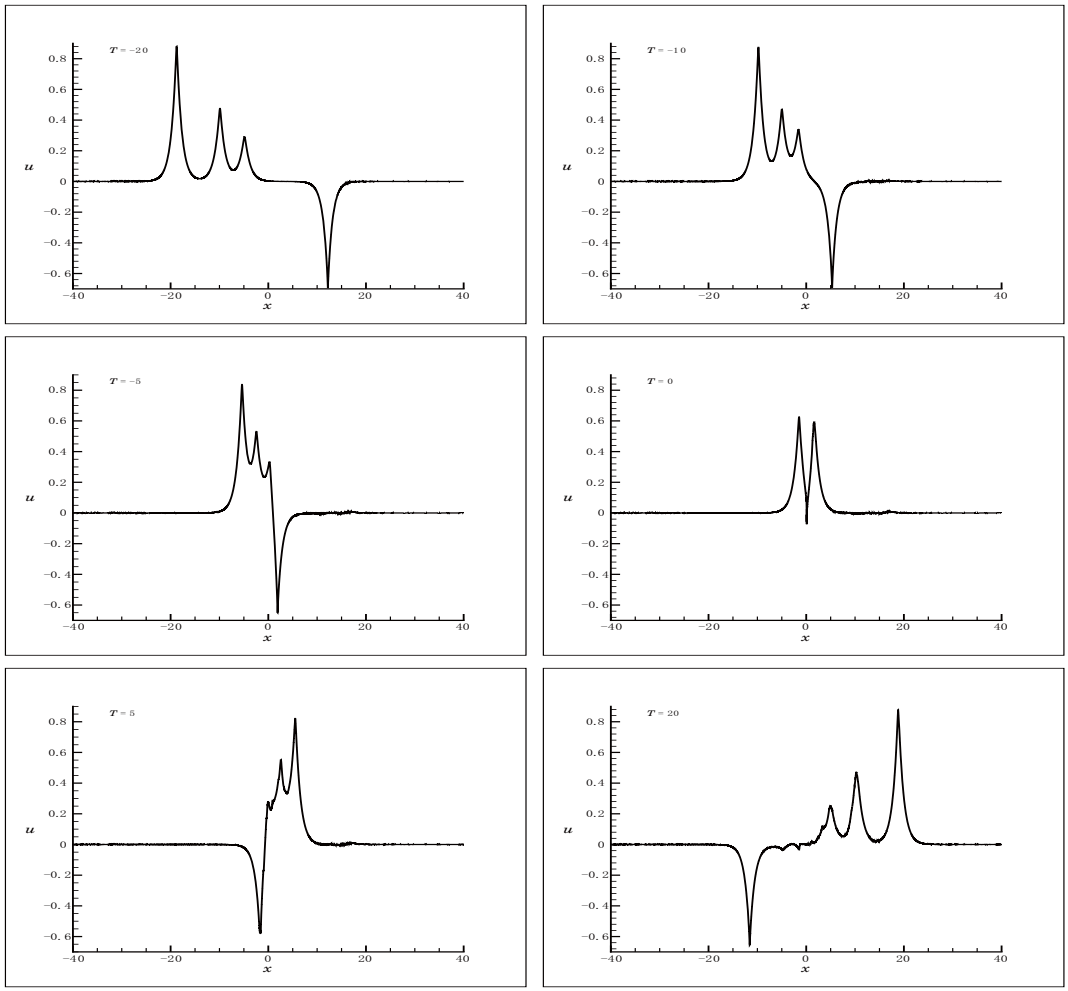


Figure 17 The interaction process of three-soliton and one cuspon solution to the CH equation (1.1) with the initial condition. Periodic boundary condition in $[-40,40]$. $P^4$ elements and a uniform mesh with 1600 cells.

with $J = 1600$ cells in our computation of the LDG method. As shown in Figure 17, we describe the interaction process of three-soliton and one-cuspon by using six different time plots. The interaction process is very similar to the result of one-soliton and three-cuspon, and the only difference is that solitons and cuspons have changed their places.

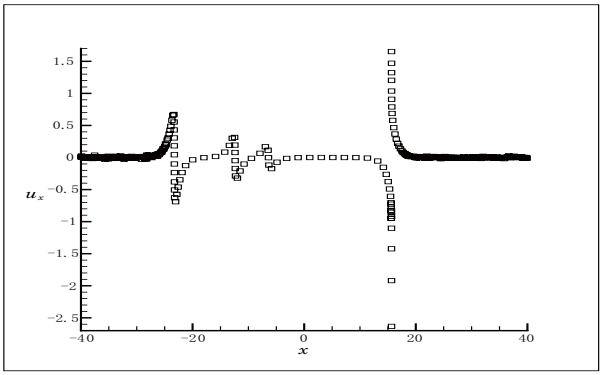


Figure 18 The function $\partial_x u(x,t)$ of three-soliton and one cuspon solution at $T = -25$.

## 5 Conclusion

In this paper, we have simulated the soliton and cuspon solution to Camassa-Holm equation by the local discontinuous Galerkin Method. First, we test and verify the theoretical results given in [7] about the phase shifts after the interactions of two-soliton, a soliton and a cuspon, two-cuspon. Finally, we find out numerical results of the phases in the interactions of three-soliton, two-soliton and a cuspon, a cuspon, a soliton and two-cuspon, three-cuspon, four-soliton, soliton and a cuspon, two-soliton and two-cuspon, a soliton and soliton and three-cuspon, four-cuspon. Try to find an arbitrary $n$-soliton and $m$-cuspon solution is more difficult, and when $n+m$ grows larger, more numerical errors (or numerical oscillation) will be introduced. So to get good plots, we have to increase the number of elements and use a higher order scheme, while each method will dramatically increase the computing cost. For this reason, we only give results with $n + m < 5$ in this paper. We expect to get results for arbitrary $n$ and $m$ with similar properties (i.e., the larger soliton (cuspon) "eats up" the smaller cuspon (soliton), the larger amplitude with faster speed, $\cdots$). And also, those numerical simulations will help us get the theoretical results about the multi-soliton and multi-cuspon solution to Camassa-Holm equation.

## References

[1] Camassa, R. and Holm, D., An integrable shallow water equation with peaked solitons, *Phys. Rev. Lett.*, **71**, 1993, 1661–1664.

[2] Camassa, R., Holm, D. and Hyman, J., A new integrable shallow water equation, *Adv. Appl. Mech.*, **31**, 1994, 1–33.

[3] Cockburn, B., Discontinuous Galerkin methods for convection-dominated problems, High-Order Methods for Computational Physics, T. J. Barth and H. Deconinck (eds.), Lecture Notes in Computational Science and Engineering, **9**, Springer-Verlag, 1999, 69–224.

[4] Cockburn, B. and Shu, C. W., TVB Runge-Kutta local projection discontinuous Galerkin finite element method for conservation laws II: general framework, *Math. Comp.*, **52**, 1989, 411–435.

[5] Cockburn, B. and Shu, C. W., Runge-Kutta discontinuous Galerkin methods for convection-dominated problems, *J. Sci. Comput.*, **16**, 2001, 173–261.

[6] Cockburn, B. and Shu, C. W., Foreword for the special issue on discontinuous Galerkin method, *J. Sci. Comput.*, **22–23**, 2005, 1–3.

[7] Dai, H. H., and Li, Y. S., The interaction of the $\omega$-soliton and $\omega$-cuspon of the Camassa-Holm equation, *J. Phys. A*, **38**, 2005, 685–694.

[8] Dawson, C., Foreword for the special issue on discontinuous Galerkin method, *Comput. Methods Appl. Mech. Engrg.*, **195**, 2006, 3183.

[9] Li, Y. S. and Zhang, J. E., The multiple-soliton solution of the Camassa-Holm equation, *Proc. R. Soc. Lond. Ser. A Math. Phys. Eng. Sci.*, **460**, 2004, 2617–2627.

[10] Li, Y. S., Some water wave equation and integrability, *J. Nonlinear Math. Phys.*, **12**, 2005, 466–481.

[11] Xu, Y. and Shu, C. W., A local discontinuous Galerkin method for the Camassa-Holm equations, *SIAM J. Numer. Anal.*, **46**, 2008, 1998–2021.

[12] Xu, Y. and Shu, C. W., Local discontinuous Galerkin method for the Hunter-Saxton equation and its zero-viscosity and zero-dispersion limit, *SIAM J. Sci. Comput.*, **31**, 2008, 1249–1268.

[13] Xu, Y. and Shu, C. W., Local discontinuous Galerkin methods for high-order time-dependent partial differential equations, *Commun. Comput. Phys.*, **7**, 2010, 1–46.

[14] Xu, Y. and Shu, C. W., Dissipative numerical methods for the Hunter-Saxton equation, *J. Comput. Math.*, **28**, 2010, 606–620.

[15] Xu, Y. and Shu, C. W., Local discontinuous Galerkin methods for the Degasperis-Procesi equation, *Commun. Comput. Phys.*, **10**, 2011, 474–508.

## Appendix The LDG Method for the Camassa-Holm Equation

To make the paper complete, the details of the LDG method for Camassa-Holm in [11] was presented in this section.

### A.1 Notation

We denote the mesh by

$$I_j = [x_{j-\frac{1}{2}}, x_{j+\frac{1}{2}}] \quad \text{for } j = 1, \cdots, N.$$

The center of the cell is

$$x_j = \frac{1}{2}(x_{j-\frac{1}{2}} + x_{j+\frac{1}{2}})$$

and the mesh size is denoted by

$$h_j = x_{j+\frac{1}{2}} - x_{j-\frac{1}{2}} \quad \text{with } h = \max_{1\le j\le N} h_j$$

being the maximum mesh size. We assume that the mesh is regular, namely, the ratio between the maximum and the minimum mesh sizes stays bounded during mesh refinement. We define the piecewise-polynomial space $V_h$ as the space of polynomials of the degree up to $k$ in each cell $I_j$, i.e.,

$$V_h = \{v : \ v \in P^k(I_j) \text{ for } x \in I_j, \ j = 1, \cdots, N\}.$$

Note that functions in $V_h$ are allowed to have discontinuities across element interfaces.

The solution of the numerical scheme is denoted by $u_h$, which belongs to the finite element space $V_h$. We denote by $(u_h)^+_{j+\frac{1}{2}}$ and $(u_h)^-_{j+\frac{1}{2}}$ the values of $u_h$ at $x_{j+\frac{1}{2}}$, from the right cell $I_{j+1}$, and from the left cell $I_j$, respectively. We use the usual notations

$$[u_h] = u_h^+ - u_h^- \quad \text{and} \quad \overline{u}_h = \frac{1}{2}(u_h^+ + u_h^-)$$

to denote the jump and the mean of the function $u_h$ at the boundary point of each element respectively.

### A.2 The LDG method

In this section, we define our LDG method for the Camassa-Holm equation (1.1), written in the following form:

$$u - u_{xx} = q, \tag{A.1}$$

$$q_t + f(u)_x = \frac{1}{2}(u^2)_{xxx} - \frac{1}{2}((u_x)^2)_x \tag{A.2}$$

with an initial condition

$$u(x, 0) = u_0(x) \tag{A.3}$$

and periodic boundary conditions

$$u(x,t) = u(x+L,t), \tag{A.4}$$

where $L$ is the period in the $x$ direction and

$$f(u) = 2\omega u + \frac{3}{2}u^2.$$

Notice that the assumption of periodic boundary conditions is for simplicity only and is not essential: the method can be easily designed for non-periodic boundary conditions.

To define the local discontinuous Galerkin method, we further rewrite (A.1) as a first order system

$$\begin{aligned} u - r_x &= q, \\ r - u_x &= 0. \end{aligned} \tag{A.5}$$

The LDG method for (A.5), where $q$ is assumed known and we have to solve for $u$, is formulated as follows: find $u_h, r_h \in V_h$ such that for all test functions $\rho, \phi \in V_h$,

$$\int_{I_j} u_h \rho \mathrm{d}x + \int_{I_j} r_h \rho_x \mathrm{d}x - (\widehat{r}_h \rho^-)_{j+\frac{1}{2}} + (\widehat{r}_h \rho^+)_{j-\frac{1}{2}} = \int_{I_j} q_h \rho \mathrm{d}x, \tag{A.6}$$

$$\int_{I_j} r_h \phi \mathrm{d}x + \int_{I_j} u_h \phi_x \mathrm{d}x - (\widehat{u}_h \phi^-)_{j+\frac{1}{2}} + (\widehat{u}_h \phi^+)_{j-\frac{1}{2}} = 0. \tag{A.7}$$

The "hat" terms in (A.6)–(A.7) in the cell boundary terms from integration by parts are the so-called "numerical fluxes", which are single valued functions defined on the edges and should be designed based on different guiding principles for different PDEs to ensure stability. For the standard elliptic equation (A.5), we can take the simple choices such that

$$\widehat{r}_h = r_h^-, \quad \widehat{u}_h = u_h^+, \tag{A.8}$$

where we have omitted the half-integer indices $j + \frac{1}{2}$ as all quantities in (A.8) are computed at the same points (i.e., the interfaces between the cells). We remark that the choice for the fluxes (A.8) is not unique. We can for example also choose the following numerical flux:

$$\widehat{r}_h = r_h^+, \quad \widehat{u}_h = u_h^-. \tag{A.9}$$

For (A.2), we can also rewrite it into a first order system

$$\begin{aligned} q_t + f(u)_x - p_x + B(r)_x &= 0, \\ p - (b(r)u)_x &= 0, \\ r - u_x &= 0, \end{aligned} \tag{A.10}$$

where

$$B(r) = \frac{1}{2}r^2, \quad b(r) = B'(r) = r.$$

Now we can define a local discontinuous Galerkin method for (A.10), resulting in the following scheme: find $q_h, p_h, r_h \in V_h$ such that for all test functions $\varphi, \psi, \eta \in V_h$,

$$\int_{I_j} (q_h)_t \varphi \mathrm{d}x - \int_{I_j} (f(u_h) - p_h + B(r_h))\varphi_x \mathrm{d}x$$
$$+ ((\widehat{f} - \widehat{p}_h + \widehat{B(r_h)})\varphi^-)_{j+\frac{1}{2}} - ((\widehat{f} - \widehat{p}_h + \widehat{B(r_h)})\varphi^+)_{j-\frac{1}{2}} = 0, \tag{A.11}$$

$$\int_{I_j} p_h \psi \mathrm{d}x + \int_{I_j} b(r_h) u_h \psi_x \mathrm{d}x - (\widehat{b(r_h)}\widetilde{u}_h \psi^-)_{j+\frac{1}{2}} + (\widehat{b(r_h)}\widetilde{u}_h \psi^+)_{j-\frac{1}{2}} = 0, \tag{A.12}$$

$$\int_{I_j} r_h \eta \mathrm{d}x + \int_{I_j} u_h \eta_x \mathrm{d}x - (\widehat{u}_h \eta^-)_{j+\frac{1}{2}} + (\widehat{u}_h \eta^+)_{j-\frac{1}{2}} = 0. \tag{A.13}$$

The numerical fluxes in (A.11)–(A.13) are chosen as

$$\widehat{p}_h = p_h^-, \quad \widehat{u}_h = u_h^+, \quad \widehat{B(r_h)} = B(r_h^-), \quad \widehat{b(r_h)} = \frac{B(r_h^+) - B(r_h^-)}{r_h^+ - r_h^-}, \quad \widetilde{u}_h = u_h^+, \tag{A.14}$$

where $\widehat{f}(u_h^-, u_h^+)$ is a monotone flux for solving conservation laws, i.e., it is Lipschitz continuous in both arguments, consistent ($\widehat{f}(u_h, u_h) = f(u_h)$), non-decreasing in the first argument and non-increasing in the second argument. Examples of monotone fluxes which are suitable for discontinuous Galerkin methods can be found in, e.g., [4]. We could, for example, use the simple Lax-Friedrichs flux

$$\widehat{f}(u_h^-, u_h^+) = \frac{1}{2}(f(u_h^-) + f(u_h^+) - \alpha(u_h^+ - u_h^-)), \quad \alpha = \max |f'(u_h)|,$$

where the maximum is taken over a relevant range of $u_h$. This Lax-Friedrichs flux is used in the numerical experiments in the next section. The definition of the algorithm is now complete.

We remark that the choice for the fluxes (A.14) is not unique. In fact, the crucial part is taking $\widehat{p}_h$ and $\widehat{u}_h$ from opposite sides and $\widehat{B(r_h)}$ and $\widetilde{u}_h$ from opposite sides.

### A.3 Algorithm flowchart

In this section, we give details related to the implementation of the method.

**Step 1** First, from (A.6)–(A.8), we obtain $q_h$ in the following matrix form:

$$\boldsymbol{q}_h = \mathbf{A}\boldsymbol{u}_h, \tag{A.15}$$

where $\boldsymbol{q}_h$ and $\boldsymbol{u}_h$ are the vectors containing the degrees of freedom for $q_h$ and $u_h$, respectively.

**Step 2** From (A.11)–(A.14), we obtain the LDG discretization of the residual $-f(u)_x + \frac{1}{2}(u^2)_{xxx} - \frac{1}{2}((u_x)^2)_x$ in the following vector form:

$$(\boldsymbol{q}_h)_t = \mathbf{res}(\boldsymbol{u}_h). \tag{A.16}$$

**Step 3** We then combine (A.15) and (A.16) to obtain

$$\mathbf{A}(\boldsymbol{u}_h)_t = \mathbf{res}(\boldsymbol{u}_h). \tag{A.17}$$

**Step 4** We use a time discretization method to solve

$$(\boldsymbol{u}_h)_t = \mathbf{A}^{-1}\mathbf{res}(\boldsymbol{u}_h). \tag{A.18}$$

This step involves a linear solver with the matrix $\mathbf{A}$. We perform an $LU$ decomposition for $\mathbf{A}$ at the beginning and use it for all time steps. Any standard ODE solvers can be used here, for example, the Runge-Kutta methods.

The LDG matrix $\mathbf{A}$ is a sparse block matrix, and hence its multiplication with vectors and a linear solver involving it as the coefficient matrix can be implemented efficiently.